

# Optimization of light delivery by a nanowire-based single cell optical endoscope

Mikhail Ladanov,<sup>1</sup> Surya Cheemalapati,<sup>1</sup> and Anna Pyayt,<sup>1,\*</sup>

<sup>1</sup>Department of Chemical and Biomedical Engineering, University of South Florida, 4202 E. Fowler Ave. Tampa, FL 33620, USA  
\*pyayt@usf.edu

**Abstract:** Here we present a new design and FDTD simulations of light delivery by a nanowire-based intracellular endoscope. Nanowires can be used for minimally invasive and very local light delivery inside cells. One of the main challenges is coupling of light into the nanowire. We propose a new plasmonic coupler interface between cleaved optical fiber and a nanowire, and optimize light coupling efficiency and contrast.

©2013 Optical Society of America

**OCIS codes:** (170.0170) Medical optics and biotechnology; (220.0220) Optical design and fabrication

---

## References and links

1. H. Andersson and A. van den Berg, "Microtechnologies and nanotechnologies for single-cell analysis," *Curr. Opin. Biotechnol.* **15**(1), 44–49 (2004).
2. J. E. Ferrell, Jr. and E. M. Machleder, "The biochemical basis of an all-or-none cell fate switch in xenopus oocytes," *Science* **280**(5365), 895–898 (1998).
3. J. S. Marcus, W. F. Anderson, and S. R. Quake, "Microfluidic single-cell mRNA isolation and analysis," *Anal. Chem.* **78**(9), 3084–3089 (2006).
4. W. J. Blake, M. KAern, C. R. Cantor, and J. J. Collins, "Noise in eukaryotic gene expression," *Nature* **422**(6932), 633–637 (2003).
5. M. B. Elowitz, A. J. Levine, E. D. Siggia, and P. S. Swain, "Stochastic gene expression in a single cell," *Science* **297**(5584), 1183–1186 (2002).
6. M. N. Teruel and T. Meyer, "Parallel single-cell monitoring of receptor-triggered membrane translocation of a calcium-sensing protein module," *Science* **295**(5561), 1910–1912 (2002).
7. S. Lindström and H. Andersson-Svahn, "Miniaturization of biological assays — Overview on microwell devices for single-cell analyses," *Biochimica et Biophysica Acta (BBA) - General Subjects* **1810**(3), 308–316 (2011).
8. B. H. Villas, "Flow cytometry: an overview," *Cell Vis.* **5**(1), 56–61 (1998).
9. P. O. Krutzik and G. P. Nolan, "Fluorescent cell barcoding in flow cytometry allows high-throughput drug screening and signaling profiling," *Nat. Methods* **3**(5), 361–368 (2006).
10. J. P. Nolan and L. A. Sklar, "The emergence of flow cytometry for sensitive, real-time measurements of molecular interactions," *Nat. Biotechnol.* **16**(1), 633–638 (1998).
11. M. Oheim, "High-throughput microscopy must re-invent the microscope rather than speed up its functions," *Br. J. Pharmacol.* **152**(1), 1–4 (2007).
12. R. Pepperkok and J. Ellenberg, "High-throughput fluorescence microscopy for systems biology," *Nat. Rev. Mol. Cell Biol.* **7**(9), 690–696 (2006).
13. Z. Orynbayeva, R. Singhal, E. A. Vitol, M. G. Schrlau, E. Papazoglou, G. Friedman, and Y. Gogotsi, "Physiological validation of cell health upon probing with carbon nanotube endoscope and its benefit for single-cell interrogation," *Nanomedicine* **8**(5), 590–598 (2012).
14. R. Singhal, Z. Orynbayeva, R. V. Kalyana Sundaram, J. J. Niu, S. Bhattacharyya, E. A. Vitol, M. G. Schrlau, E. S. Papazoglou, G. Friedman, and Y. Gogotsi, "Multifunctional carbon-nanotube cellular endoscopes," *Nat. Nanotechnol.* **6**(1), 57–64 (2011).
15. R. Yan, J.-H. Park, Y. Choi, C.-J. Heo, S.-M. Yang, L. P. Lee, and P. Yang, "Nanowire-based single-cell endoscopy," *Nat. Nanotechnol.* **7**(3), 191–196 (2011).
16. X. Chen, A. Kis, A. Zettl, and C. R. Bertozzi, "A cell nanoinjector based on carbon nanotubes," *Proc. Natl. Acad. Sci. U.S.A.* **104**(20), 8218–8222 (2007).
17. K. Yum, S. Na, Y. Xiang, N. Wang, and M.-F. Yu, "Mechanochemical delivery and dynamic tracking of fluorescent quantum dots in the cytoplasm and nucleus of living cells," *Nano Lett.* **9**(5), 2193–2198 (2009).
18. R. Singhal, S. Bhattacharyya, Z. Orynbayeva, E. Vitol, G. Friedman, and Y. Gogotsi, "Small diameter carbon nanopipettes," *Nanotechnology* **21**(1), 015304 (2010).

19. S. Han, C. Nakamura, I. Obataya, N. Nakamura, and J. Miyake, "Gene expression using an ultrathin needle enabling accurate displacement and low invasiveness," *Biochem. Biophys. Res. Commun.* **332**(3), 633–639 (2005).
20. G. Shambat, S.-R. Kothapalli, J. Provine, T. Sarmiento, J. Harris, S. S. Gambhir, and J. Vučković, "Single-cell photonic nanocavity probes," *Nano Lett.* DOI: 10.1021/nl304602d (2013).
21. J. J. Niu, M. G. Schrlau, G. Friedman, and Y. Gogotsi, "Carbon nanotube-tipped endoscope for in situ intracellular surface-enhanced Raman spectroscopy," *Small* **7**(4), 540–545 (2011).
22. E. A. Vitol, Z. Orynbayeva, M. J. Bouchard, J. Azizkhan-Clifford, G. Friedman, and Y. Gogotsi, "In situ intracellular spectroscopy with Surface Enhanced Raman Spectroscopy (SERS)-enabled nanopipettes," *ACS Nano* **3**(11), 3529–3536 (2009).
23. A. L. Pyayt, B. Wiley, Y. Xia, A. Chen, and L. Dalton, "Integration of photonic and silver nanowire plasmonic waveguides," *Nat. Nanotechnol.* **3**(11), 660–665 (2008).
24. M. Law, D. J. Sirbuly, J. C. Johnson, J. Goldberger, R. J. Saykally, and P. Yang, "Nanoribbon waveguides for subwavelength photonics integration," *Science* **305**(5688), 1269–1273 (2004).
25. D. J. Sirbuly, M. Law, P. Pauzauskie, H. Yan, A. V. Maslov, K. Knutsen, C.-Z. Ning, R. J. Saykally, and P. Yang, "Optical routing and sensing with nanowire assemblies," *Proc. Natl. Acad. Sci. U.S.A.* **102**(22), 7800–7805 (2005).
26. P. M. Kasili, J. M. Song, and T. Vo-Dinh, "optical sensor for the detection of caspase-9 activity in a single cell," *J. Am. Chem. Soc.* **126**(9), 2799–2806 (2004).
27. W. Tan, Z. Y. Shi, S. Smith, D. Birnbaum, and R. Kopelman, "Submicrometer intracellular chemical optical fiber sensors," *Science* **258**(5083), 778–781 (1992).
28. T. Vo-Dinh, J.-P. Alarie, B. M. Cullum, and G. D. Griffin, "Antibody-based nanoprobe for measurement of a fluorescent analyte in a single cell," *Nat. Biotechnol.* **18**(7), 764–767 (2000).
29. T. Vo-Dinh and P. Kasili, "Fiber-optic nanosensors for single-cell monitoring," *Anal. Bioanal. Chem.* **382**(4), 918–925 (2005).
30. J. Chen, F. Saeki, B. J. Wiley, H. Cang, M. J. Cobb, Z.-Y. Li, L. Au, H. Zhang, M. B. Kimmey, X. Li, and Y. Xia, "Gold Nanocages: Bioconjugation and Their Potential Use as Optical Imaging Contrast Agents," *Nano Lett.* **5**(3), 473–477 (2005).
31. J. Chen, D. Wang, J. Xi, L. Au, A. Siekkinen, A. Warsen, Z.-Y. Li, H. Zhang, Y. Xia, and X. Li, "Immuno gold nanocages with tailored optical properties for targeted photothermal destruction of cancer cells," *Nano Lett.* **7**(5), 1318–1322 (2007).
32. P. J. Campagnola and L. M. Loew, "Second-harmonic imaging microscopy for visualizing biomolecular arrays in cells, tissues and organisms," *Nat. Biotechnol.* **21**(11), 1356–1360 (2003).
33. P. J. Campagnola, A. C. Millard, M. Terasaki, P. E. Hoppe, C. J. Malone, and W. A. Mohler, "Three-dimensional high-resolution second-harmonic generation imaging of endogenous structural proteins in biological tissues," *Biophys. J.* **82**(1), 493–508 (2002).
34. R. LaComb, O. Nadiarnykh, and P. J. Campagnola, "Quantitative second harmonic generation imaging of the diseased state osteogenesis imperfecta: Experiment and simulation," *Biophys. J.* **94**(11), 4504–4514 (2008).
35. N. S. Makarov, E. Beuerman, M. Drobizhev, J. Starkey, and A. Rebane, "Environment-sensitive two-photon dye," *Proc. SPIE* **7049**, 70490Y, 70490Y-12 (2008).
36. J. R. Starkey, N. S. Makarov, M. Drobizhev, and A. Rebane, "Highly sensitive detection of cancer cells using femtosecond dual-wavelength near-IR two-photon imaging," *Biomed. Opt. Express* **3**(7), 1534–1547 (2012).
37. A. Petrušis, J. H. Rector, K. Smith, S. Man, and D. Iannuzzi, "The align-and-shine technique for series production of photolithography patterns on optical fibres," *J. Micromech. Microeng.* **19**(4), 047001 (2009).
38. P.-C. Chang, Z. Fan, D. Wang, W.-Y. Tseng, W.-A. Chiou, J. Hong, and J. G. Lu, "ZnO Nanowires Synthesized by Vapor Trapping CVD Method," *Chem. Mater.* **16**(24), 5133–5137 (2004).
39. M. H. Huang, Y. Wu, H. Feick, N. Tran, E. Weber, and P. Yang, "Catalytic Growth of Zinc Oxide Nanowires by Vapor Transport," *Adv. Mater.* **13**(2), 113–116 (2001).
40. M. Kirkham, X. Wang, Z. L. Wang, and R. L. Snyder, "Solid Au nanoparticles as a catalyst for growing aligned ZnO nanowires: a new understanding of the vapour–liquid–solid process," *Nanotechnology* **18**(36), 365304 (2007).
41. L. E. Greene, M. Law, J. Goldberger, F. Kim, J. C. Johnson, Y. Zhang, R. J. Saykally, and P. Yang, "Low-Temperature Wafer-Scale Production of ZnO Nanowire Arrays," *Angew. Chem. Int. Ed. Engl.* **42**(26), 3031–3034 (2003).
42. L. E. Greene, M. Law, D. H. Tan, M. Montano, J. Goldberger, G. Somorjai, and P. Yang, "General route to vertical ZnO nanowire arrays using textured ZnO seeds," *Nano Lett.* **5**(7), 1231–1236 (2005).
43. L. Vayssieres, "Growth of arrayed nanorods and nanowires of ZnO from aqueous solutions," *Adv. Mater.* **15**(5), 464–466 (2003).
44. T. W. Ebbesen, H. J. Lezec, H. F. Ghaemi, T. Thio, and P. A. Wolff, "Extraordinary optical transmission through sub-wavelength hole arrays," *Nature* **391**(6668), 667–669 (1998).
45. F. Miyamaru and M. Hangyo, "Anomalous terahertz transmission through double-layer metal hole arrays by coupling of surface plasmon polaritons," *Phys. Rev. B* **71**(16), 165408 (2005).
46. M. G. Velasco, P. Cassidy, and H. Xu, "Extraordinary transmission of evanescent modes through a dielectric-filled nanowaveguide," *Opt. Commun.* **284**(19), 4805–4809 (2011).

## 1. Introduction

A single cell response to a stimulus can be quite different from an average response of a cell colony [1]. This difference can be caused by variety of reasons including the phase of cell division [2], stochasticity, or noise, in gene expression [3–5], ion concentrations [6] and many others. Therefore, the analysis on a single cell level may provide much more complete picture with important details normally missed when studying cell culture. Additionally, the data obtained from a single cell study are required for better understanding of biochemical processes inside the cell.

Over the time different methods for a single cell analysis have been developed [7]. Some of the most commonly used techniques are flow cytometry (FC) [8], fluorescence-activated cell sorting (FACS) [9, 10], automated (AM) and high-throughput microscopy (HTM) [11, 12]. However, recently new nanotechnology based approaches emerged and immediately attracted a lot of attention because of unique capability to deliver exogenous payloads into cells and perform high spatial resolution spectral study inside the cell. One of the main advantages of these methods is use of nanoscale probes capable of safe penetration through the cell membrane without causing death or apoptosis [13]. The methods currently being developed include intracellular electrochemical measurements [14] and photocatalytic [15] or mechanochemical [16, 17] payload delivery. Additionally, variety of nanomechanical tools for payload delivery into the cell were introduced, including a nanoinjector based on a carbon nanopipets [18] or carbon nanotubes being a part of multiwalled carbon nanotube (MWCNT) attached to an atomic force microscope (AFM) tip [16], or just an AFM tip turned into a nanoneedle using FIB [19]. Furthermore, the following innovative tools for optical probing of the cells have been developed: nanowire-based endoscope [15], endoscope based on a photonic crystal [20], and SERS-enabled endoscope [14, 21, 22]. In those devices light propagating in the nanowire can trigger a photoactive process for payload delivery by cutting off photocleavable linkers or can be used for high resolution intracellular spectroscopy. Critical steps required for realization of such instruments are coupling of light into nanowires [23–25] and sensing at the nanoscale [26–29]. Additionally, fluorescence combined with nanowire-based endoscopy can be used not only to deliver light in the cell, but also to pick up the signal from the locally excited quantum dots [15]. The advantages of the nanowire-based design are very small excitation volume and less invasive penetration through the cell membrane, allowing study of photosensitive processes inside of a living cell.

In order to make transition from the single use experimental tools demonstrating the principle to more standard device configuration suitable for mass-production and application in biomedical research labs, a much better understanding of the design principles at the nanoscale is required. Specifically, for the nanoscale endoscopes, predictable and controllable interface between the nanowire and the macroscopic world has to be developed. Ideally light should be coupled from a regular optical fiber, so this requires creation of a structure that would couple light from the optical mode propagating in the fiber into the optical mode that propagates in the nanowire. Even though some complex structures requiring manual assembly were developed [15], there is a need to make alternative design suitable for mass production. The requirements would be to minimize manual assembly and use standard techniques of Microelectromechanical systems (MEMS) fabrication together with traditional nanowire growth procedures. Additional set of constraints comes from the need to couple light well into the nanowire while minimizing the background exposure decreasing imaging contrast. Therefore we propose a new design of the nanoscale endoscope suitable for mass production as described in the next section. A FDTD simulation utilizing proposed design of light propagation through the endoscope was carried out. The simulation is primarily concentrated on the light delivery rather than on light measurement since there are number of applications that only require light delivery through the endoscope, while light collection can be done through the microscope objective [15, 30, 31].

Ultra-high resolution imaging of the cell interior can be done by 3D-scanning the nano-endoscope with very small step (20-40 nm are easily attainable by contemporary micromanipulators). Camera designed for visible light and near IR light will not detect 1550 nm excitation light, while second harmonic generation or two photon imaging can be realized detected using a camera attached to a microscope [32–36].

## 2. Design

The pioneering device demonstrated by Peydong Yang's lab [15] was using nanowires manually glued to the thinned fiber. For this configuration it is hard to predict efficiency of coupling as well as other parameters of the endoscope such as mechanical robustness and effects of diffraction of light at the tip of the fiber on the overall device performance. Here we propose an alternative approach that would simplify the manufacturing process, at the same time giving more broad control over the distribution of light intensity in the vicinity of the nanoprobe tip. The suggested design does not require thinning of the fiber core, instead, a thin metal ring can be patterned on the cleaved tip of the fiber for the selective coupling of the light from the fiber core to the nanowire as shown in Fig. 1. Focused Ion Beam (FIB) can be used to pattern a circular opening in thin metal layer deposited on the fiber tip. Just single use of FIB is required, and then the design can be reproduced on many fibers using *align-and-shine* photolithography process [37]. The nanowire can be directly grown in the opening using one of many gas [38–40] and hydrothermal [41–43] nanowire growth techniques. Overall proposed design significantly increases the reliability and ease of production, offering unprecedented control over the light field.

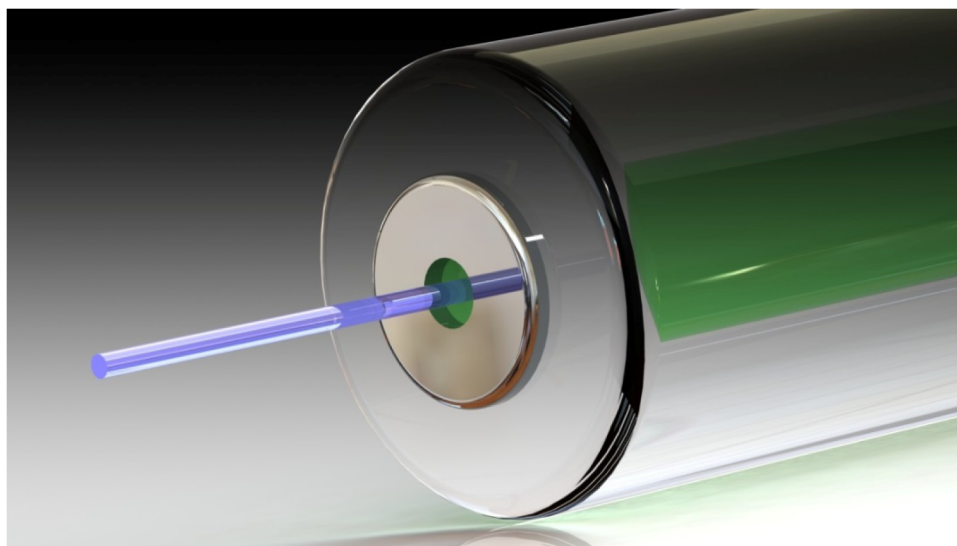


Fig. 1. Schematics of the proposed design of the new nanowire-based single cell endoscope (not to scale). First, thin film of metal is deposited on the cleaved fiber interface covering the core of the fiber. Then, an opening is milled in the center of the fiber interface using FIB. The purpose of the metal protection is to prevent light leakage and to optimize coupling of the light into the nanowire. Finally, the nanowire is grown directly in the opening of the fiber.

Figure 2 demonstrates modes propagating in the optical fiber and the nanowire used in the simulations. The two left images are the side view of the field distribution in the nanowire (top) and the fiber (bottom). Right images show a cross section of the mode coupled in the nanowire (top) and the fiber (bottom). It can be seen that the sizes of the modes are very different and that for the nanowire large portion of energy is concentrated around the nanowire.

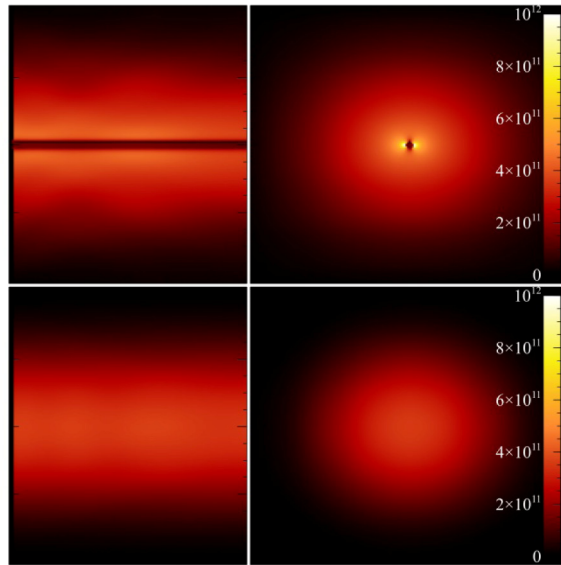


Fig. 2. Mode propagating in the nanowire (top) and the optical fiber (bottom). Side view (left) and cross-section (right) are shown.

### 3. Simulation

Three-dimensional simulations were performed on commercial FDTD software. The design parameters were: wavelength  $1.5 \mu\text{m}$ , single mode optical fiber with refractive index 1.46 and  $8 \mu\text{m}$  core diameter, layer of metal on the tip of the fiber with thickness of 200nm. An opening was located in the center of the metal film with the radius that was varied between 0.1 and  $3.0 \mu\text{m}$ . A nanowire made of ZnO with refractive index of 2, diameter of 200 nm and length of  $2 \mu\text{m}$  was placed in the center of the opening at the end of the fiber. Light was propagating in the fiber and then coupled to the nanowire. The efficiency of coupling varied depending on the radius of the opening in the metal.

### 4. Results

Distributions of electric field amplitude were measured in the plane that was parallel to the initial polarization of the coupled mode and the optical axis of the fiber. To estimate the contribution into field distribution introduced by the nanowire, initial simulations were performed for a configuration that did not have nanowire (Fig. 3(a)) and then the nanowire was added (Fig. 3(b)). Opening in the metal layer had radius  $\delta$  ranging from  $0.2 \mu\text{m}$  to  $2.8 \mu\text{m}$ . Afterwards, a direct difference of the field amplitudes were calculated to estimate the contribution of the mode coupled into the nanowire into the total field distribution around the nanowire (Fig. 4(a)). Division of the simulated field intensity of configuration containing nanowire by the field intensity of configuration without nanowire were used to estimate the effect of local field enhancement introduced by the nanowire (Fig. 4(b)). While division provides information about relative intensity, difference describes absolute value that can be relatively small for the openings with the smaller radius.

First of all, it can be noticed that in absence of the nanowire (Fig. 3(a)) there is a cut off radius of the opening in the metal ( $\sim 0.8 \mu\text{m}$ ) after which light does not escape the fiber, exhibiting evanescent behavior. With larger openings a typical field distribution of diffraction on an opening can be observed.

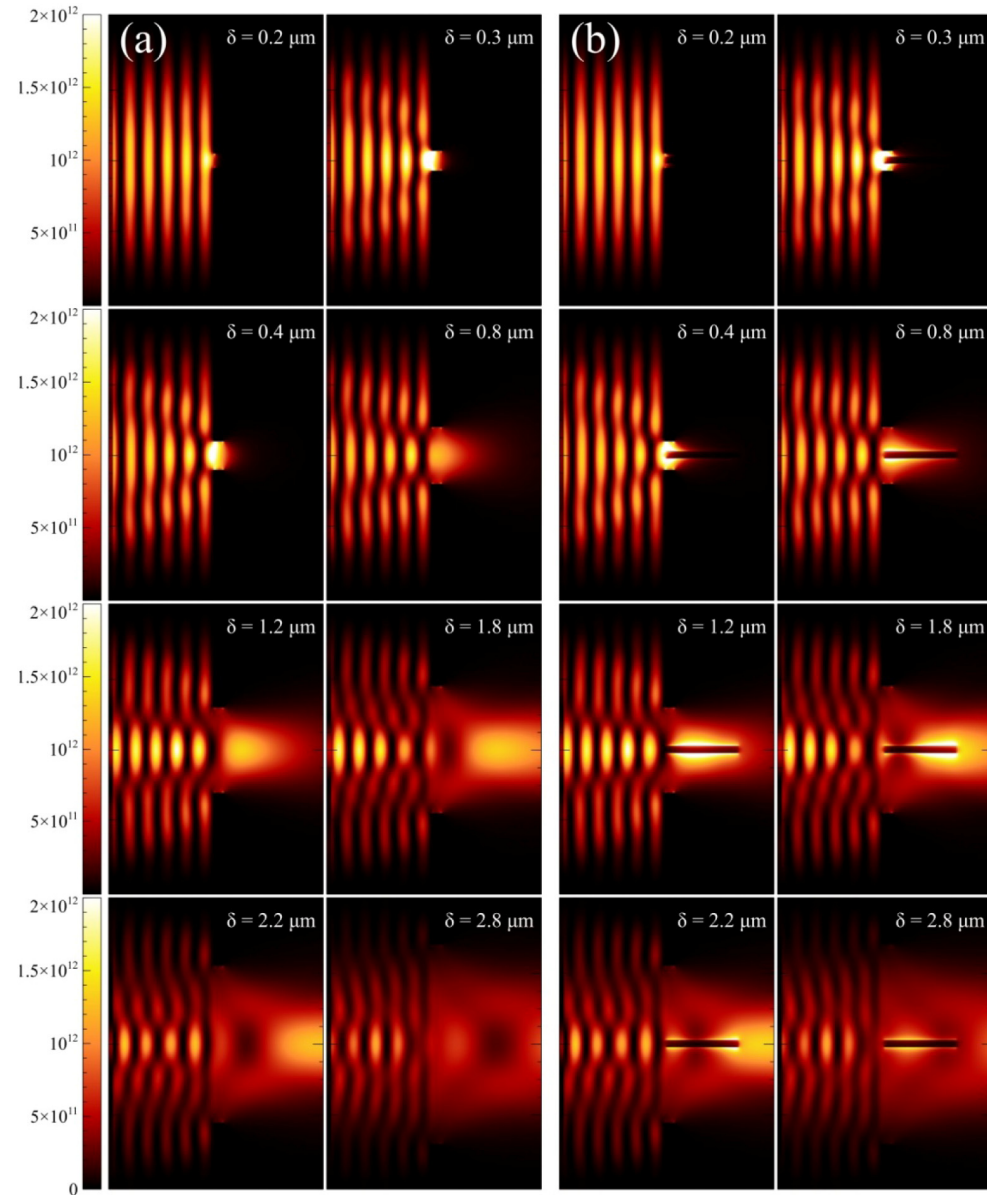


Fig. 3. Simulation of the light propagation outside of the optical fiber through the metal opening when the nanowire is absent (a) and present (b). Each section demonstrates light intensity distribution in cross-section of the system demonstrated in Fig. 1. The left side of each individual section corresponds to the light propagating in the core of optical fiber, thin metal layer (not visible) with opening is located in the center of the section, while the right part of the section corresponds to the light propagating through the opening out of the fiber core with (b) or without (a) the nanowire.

Next, when the nanowire is added to the system the field distribution outside of the optical fiber changes significantly (Fig. 3(b)). It can be observed that even for the openings in metal with a radius smaller than cut off radius, light propagates by coupling into the nanowire. When the radius of the opening is increased, it reaches the point when light couples into the nanowire only partially, with some amount of the light propagating in the space around the nanowire. This was investigated further in Fig. 4(a) showing difference in the field amplitude

when nanowires were present and absent. Dark red corresponds to zero difference, while brighter areas indicate that the field in the configuration with nanowire is higher than that in the configuration without it, vice versa, darker areas indicate that the fields without nanowire in that area is higher. Figure 4(b) illustrates the ratio of the corresponding intensities. It can be observed that for the opening  $0.2\ \mu\text{m}$  extremely low light propagation is observed outside of the optical fiber.

For the opening with  $0.3$  and  $0.4\ \mu\text{m}$  radius there are two observations. First, light is locally enhanced in the metal opening due to plasmonic effects. Abnormally high propagation through sub-microne holes has been observed previously experimentally and theoretically [44–46], which comes in good agreement with these simulations. Second, outside of the metal opening light propagates along the nanowire in a uniform mode with the field concentrated closely around the nanowire in a way similar to the mode supported by the nanowire shown in Fig. 2.

For larger openings presence of the nanowire has changed propagation of the light outside of the optical fiber. First of all, Fig. 4(a) showing the difference of the fields in presence/absence of the nanowire demonstrates that the field around the nanowire is locally enhanced. There are two possible mechanisms explaining this effect. One of them is coupling of the light into nanowire and propagation it outside of the optical fiber. Second is a local field enhancement purely related to the difference in refractive indices between air and ZnO. The ratio of the influence of those two mechanisms can be extracted from comparison of the subtraction and division of the fields with and without nanowires (Fig. 4(a) and (b)). It can be noticed that for larger openings presence of the nanowire causes uniform field enhancement along the nanowire (Fig. 4(b)), even when the field itself is not uniform (Fig. 3(a)). This indicates domination of the local field enhancement, since the nanowire mode is much more uniform along its length. There is a well defined region around the nanowire with field enhanced two-times or more, which is in good agreement with results theoretically expected based on refractive indices difference.

When the radius of the opening decreases below  $0.8\ \mu\text{m}$ , the ratio of light intensity in the area around the nanowire to the intensity without nanowire is getting higher with the decrease of the opening (Fig. 4(b)). It can be explained by significantly less light escaping the fiber through the opening in the metal film without coupling into nanowire, thus light propagation by coupling into the nanowire starts playing more important role.

To finalize, in order to deliver light using this nanoscale single cell endoscope inside the cell in close proximity to the organelles of interest light has to propagate along the nanowire. To achieve high resolution scanning of the cell interior light has to be present in a small excitation volume. There is trade-off between two different configurations. If high contrast is extremely important, the best way is to create small opening in the metal layer. Light from the whole area of the opening will be coupled into mode supported by the nanowire while non-coupled light leakage around the nanowire will be minimized. It was shown that the coupling is optimal, and the excitation volume is minimal with the radius of the metal opening  $0.4\ \mu\text{m}$ . If the background light is not too critical, but local intensity is the most important, then openings between  $0.4$  and  $0.8\ \mu\text{m}$  would provide enough light outside of the optical fiber than would be locally enhanced by the nanowire. Openings larger than  $0.8\ \mu\text{m}$  just create additional background increasing the level of noise.

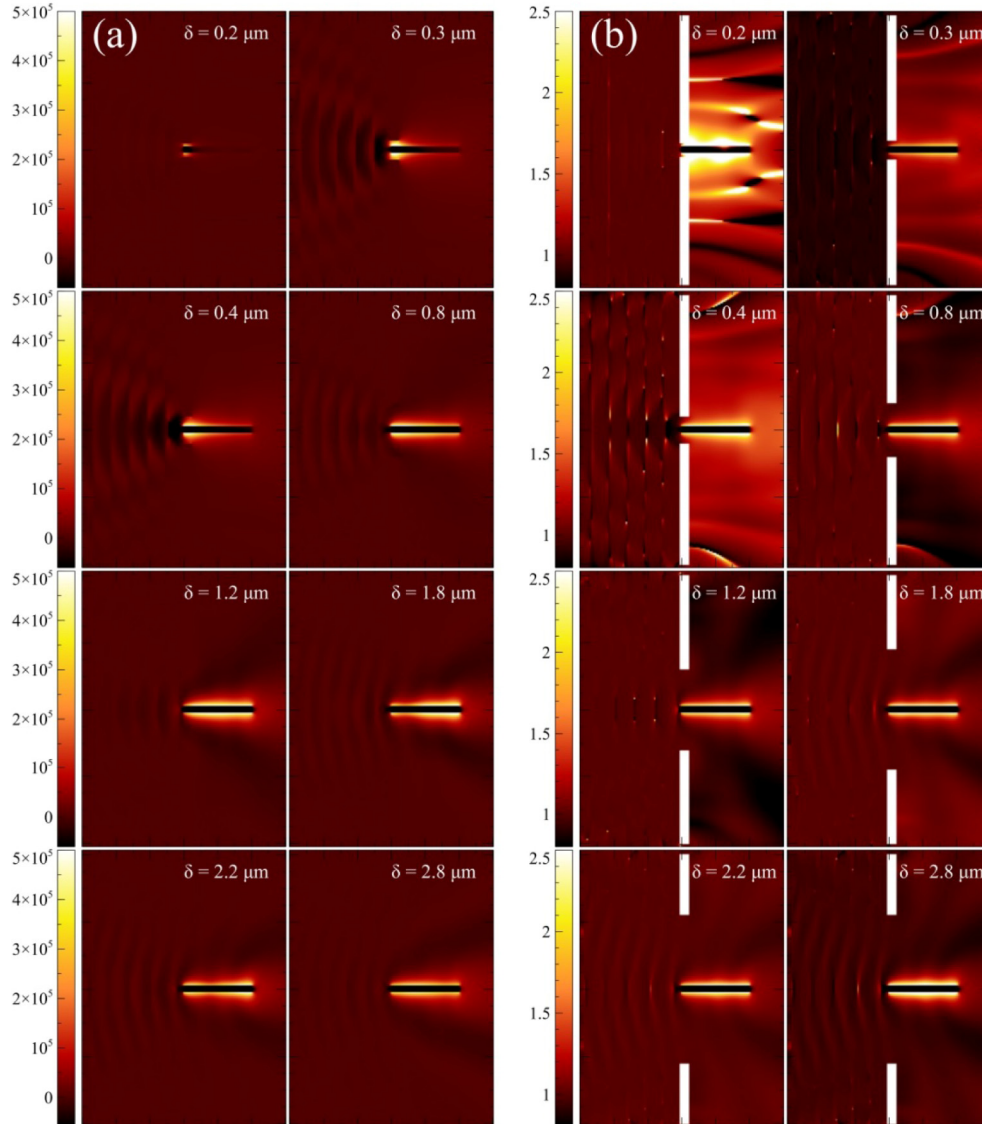


Fig. 4. (a) Calculated difference between field amplitude distribution with and without the nanowire. (b) Normalized light intensity distribution. Light intensity of the configuration with the nanowire was divided by the light intensity of the configuration without the nanowire. Top two images show some calculation artifacts since for the areas far from the center the field without nanowire is almost zero. Therefore, normalization relative to the almost zero fields significantly magnifies very low differences. In areas around nanowires the field is always present, therefore the normalization is not sensitive to artifact.

## 5. Conclusion

A new design and FDTD simulations for a nanowire-based intracellular endoscope are presented based on a combination of an optical fiber and a nanowire. The fiber can be used as is, freshly cleaved, without applying any thinning techniques. A thin film of a metal deposited on the tip of the fiber and then milled aids better coupling of light into the nanowire and focusing of light in the vicinity of the tip of the nanowire, effectively decreasing excitation volume and increasing power density.

Series of simulations were performed in three dimensions, the resulting distribution of electric field was analyzed to determine the optimal conditions at which better coupling of light from the fiber to the nanowire occurs. Also, the distribution of field amplitude and intensity was analyzed in terms of local contrast vs. total light intensity in close proximity to the nanowire. Conditions, optimal for two possible scenarios of measurement (maximized contrast, maximized local intensity) were determined. It was observed, that with opening of subwavelength size the light transmission through the opening was either low or negligible depending on the size of the opening. Local field enhancement was observed inside the opening in the metal due to plasmonic enhancement [44, 46]. With introduction of the nanowire to the simulated configuration the light starts propagating through the nanowire, providing high contrast in the vicinity of the tip of the nanowire. It was shown that the coupling is optimal, and the excitation volume is minimal with the radius of the metal opening to be 0.4  $\mu\text{m}$ .

To summarize, the proposed instrument platform gives a researcher a flexible tool for future intracellular study, specifically for high spatial resolution intracellular spectroscopy where high local contrast is required, and photo-activated payload delivery, where maximum power delivered inside the cell is critical.